NANO LETTERS

2007
Vol. 7, No. 11
3285−3289

Tribological Properties of Densely Packed Vertically Aligned Carbon Nanotube Film on SiC Formed by Surface Decomposition

Koji Miyake,*,† Michiko Kusunoki,‡,⊥ Hatsuhiko Usami,§ Noritsugu Umehara,|| and Shinya Sasaki†,#

Advanced Manufacturing Research Institute (AMRI), National Institute of Advanced Industrial Science and Technology (AIST), 1-2-1 Namiki, Tsukuba, Ibaraki 305-8564, Japan, Japan Fine Ceramics Center, 2-4-1 Mutsuno, Atsuta-ku, Nagoya 456-8587, Japan, Faculty of Science and Engineering, Meijo University, 1-501 Shiogamaguchi, Tempaku, Nagoya 468-8502, Japan, and Department of Mechanical Science and Engineering, Graduate School of Engineering, Nagoya University, Furo-cho, Chikusa-ku, Nagoya 464-8603, Japan

Received June 18, 2007; Revised Manuscript Received September 4, 2007

ABSTRACT

Characteristic tribological properties, such as nonlinearity of the friction force–normal load curve, high coefficient of friction, and good wear-resistant performance were observed on densely packed, vertically aligned carbon nanotubes (CNTs) with different diameters and lengths using atomic force microscopy. Shorter and thicker CNTs were found to have higher coefficients of friction. The observed properties were attributed to the nonlinear elastic property of the CNTs caused by buckling.

Since their discovery,[1] carbon nanotubes (CNTs) have attracted considerable attention and stimulated intense study. Both experimental[2−6] and theoretical[7] studies have suggested that CNTs are remarkably resilient, sustaining extreme strain with no signs of brittleness, plasticity, or atomic rearrangements. Each shape change corresponds to an abrupt release of energy and a singularity in the stress−strain curve. Moreover, CNTs have excellent mechanical properties. They have extremely high Young's modulus values of more than 1000 GPa[2,3,8−10] and high tensile strength values of about 10−50 GPa,[10,11] which more than 20 times the tensile strength of typical high-strength steels. These excellent properties of CNTs offer high technological potential in materials science and microelectronics and as elements of microelectromechanical systems. CNTs have been widely used as composite materials to reinforce the original bulk materials.[12,13] However, there are few reports about the application of macroscopic forms of CNTs, which can utilize the intrinsic mechanical properties of individual CNTs.

Vertically aligned carbon nanotube (VACNT) film is considered to be a promising candidate for innovative tribomaterials. This is because high wear resistance and nonlinear frictional properties are expected from the characteristic mechanical properties of individual CNTs. However, macroscopic forms of CNTs lose the intrinsic properties of individual CNTs. For example, a CNT forest[14−17] is an example of vertically aligned CNT films, but it is known that forests are fragile. Therefore, CNT forests are not suitable for tribomaterials. Recently, some research groups have investigated the frictional properties of VACNT films.[18,19] VACNT films exhibit high coefficients of friction, while other carbon-based materials, such as graphite,[20] C_{60},[21] diamond-like carbon (DLC),[22] and carbon nitride film (CN_x),[23] have very low friction coefficients. These studies have concluded that the bending of CNTs is a major cause of the extremely high coefficient of friction of VACNT film.[18] In addition, Dickrell et al. have demonstrated the orientation dependence of CNT frictional properties.[19] CNTs exhibit consistently high friction for vertically aligned film and very low friction for CNTs aligned flat on the contact

* Corresponding author. E-mail: koji-miyake@aist.go.jp.
† AMRI, AIST.
‡ Japan Fine Ceramics Center.
§ Meijo University.
|| Nagoya University.
⊥ Present address: Division of Environmental Research, EcoTopia Science Institute, Nagoya University, Furo-cho Chikusa-ku, Nagoya 464-8603, Japan.
Present address: Department of Mechanical Engineering, Tokyo University of Science, 1-14-6 Kudankita, Chiyoda-ku, Tokyo 102-0073 Japan.

10.1021/nl0714482 CCC: $37.00
Published on Web 10/11/2007

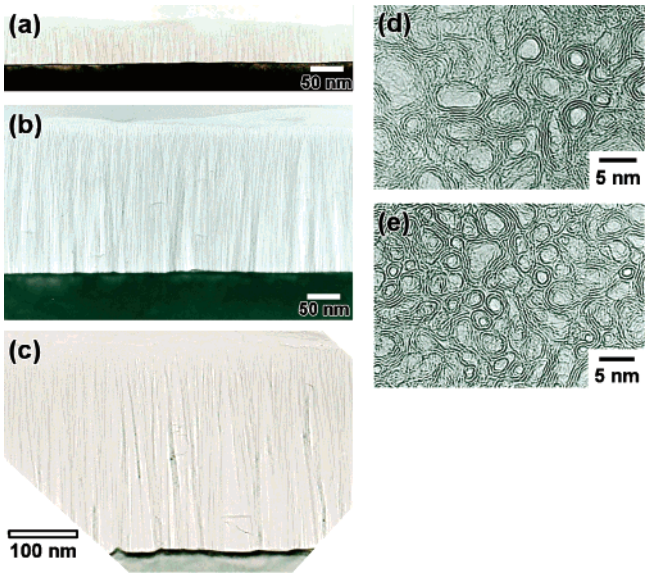

Figure 1. Cross-sectional TEM images of (a) CNT-1, (b) CNT-2, and (c) CNT-3. Plane-view TEM images of CNT diameters of (d) 5 nm and (e) 3 nm.

plane. This behavior offers the potential to control the friction force by changes in the orientation of the CNTs. These results suggest that VACNT film is a promising candidate for macroscopic forms of CNTs for tribological applications. However, these studies have not discussed the wearing of VACNT films. The wear resistance of VACNTs is an important issue for tribological applications. In these experiments, VACNT films were prepared by chemical vapor deposition (CVD) on Si(100)[18] or quartz[19] substrates. CNTs grown by CVD are only physisorbed on the substrate. Therefore, the bonding between the CNTs and the substrate can be expected to be not so strong. This problem severely affects their practical use. Furthermore, the effects of the intrinsic mechanical properties of CNTs on the frictional properties of VACNT films are still unclear. For this reason, the effects of the CNT length and diameter on their frictional properties need to be clarified on a nanoscale.

Kusunoki et al. have shown a new method for growing an aligned CNT film that is self-organized by surface decomposition on silicon carbide (SiC).[24] This method enables covalently bonded VACNT films to be grown on SiC substrate (CNT/SiC). CNT/SiC can obviate the problem of wear resistance for CNTs grown by CVD. Therefore, we consider CNT/SiC to be a promising candidate for macroscopic forms of CNTs that can utilize the intrinsic mechanical properties of individual CNTs.

This paper reports on our nanoscale evaluation of the relationships between the frictional properties and the structure of CNTs using atomic force microscopy (AFM). To confirm the effect of the CNT shape on its frictional properties, we used three CNT/SiC samples of different lengths and diameters. We also used highly oriented pyrolytic graphite (HOPG) for comparison.

The approximate lengths and diameters of each CNT were 50 and 5 nm for CNT-1, 210 and 3 nm for CNT-2, and 350 and 5 nm for CNT-3. Figure 1 shows cross-sectional

Table 1. Samples Used in the Experiments

	CNT-1	CNT-2	CNT-3	HOPG
material	CNT/SiC			graphite
length	50 nm	210 nm	300 nm	
diameter	5 nm	3 nm	5 nm	

transmission electron microscope (TEM) images of (a) CNT-1, (b) CNT-2, and (c) CNT-3. Plane-view TEM images of CNT diameters of (d) 5 nm and (e) 3 nm are also shown in Figure 1. The lengths and diameters of each CNT/SiC sample were evaluated from TEM images as shown in Figure 1. The data are summarized in Table 1. AFM images were used to analyze the frictional properties and the wear characteristics of the samples. All AFM observations were performed in air at room temperature using a V-shaped silicon nitride cantilever, with a spring constant of about 0.12 N/m for deflection and about 130 N/m for torsion. The radius of curvature of the tip we used was about 20 nm (manufacturer's specification). We varied the normal load from about 10 to 100 nN. The sliding velocity was 500 nm/s, and the sliding distance was 1 μm. Assuming the Young's modulus of the CNT is about 1 TPa,[2,3,8−10] the contact pressure during our experiments was estimated to be about 1−3 GPa.

Figure 2 shows the frictional properties of (a) HOPG, (b) CNT-1, (c) CNT-2, and (d) CNT-3 obtained under ambient conditions. For HOPG, the friction force was proportional to the normal load. From this linear relationship, the friction coefficient was evaluated to be about 0.04. This value was comparable with the value evaluated by macroscopic friction measurement. On the other hand, the frictional properties of the CNTs were clearly different from those of the HOPG.

Characteristic frictional properties were observed for the CNTs. The normal load dependence on the friction force of a CNT consists of three stages: an initial nonlinear increase, followed by a sudden drop in the slope or the curve becoming flat, and a third stage linear increase. In the third stage, a sudden drop in the friction force was observed for CNT-1 as shown in Figure 2b. Each triangle indicates singular points of each friction force−normal load curve. However, these characteristics were not observed in CNT-2, CNT-3, and the macroscopic measurement of the frictional properties of VACNT film forests.[18,19] In comparison with previous results of VACNT film forests,[18,19] we used AFM to evaluate the relationships between the frictional properties and the structure of CNTs on a nanoscale. In addition, the length of CNTs was much shorter than that of VACNT film forests.[18,19] We considered that the properties we observed were caused by the intrinsic mechanical properties of the CNTs. Next, we discuss the origin of the characteristic frictional properties of CNTs with regard to the structural change of CNTs.

It is well-known that CNTs subject to large deformations change into different morphological patterns.[2−6] Each shape change corresponds to an abrupt release of energy and a singularity in the stress−strain curve.[7] In addition, it is also predicted that the abrupt change in the curve slope corresponds to an elastic process. Single- and double-wall CNTs buckle elastically to yield a structure reminiscent of that formed when a macroscopic rubber tube is bent and kinked.

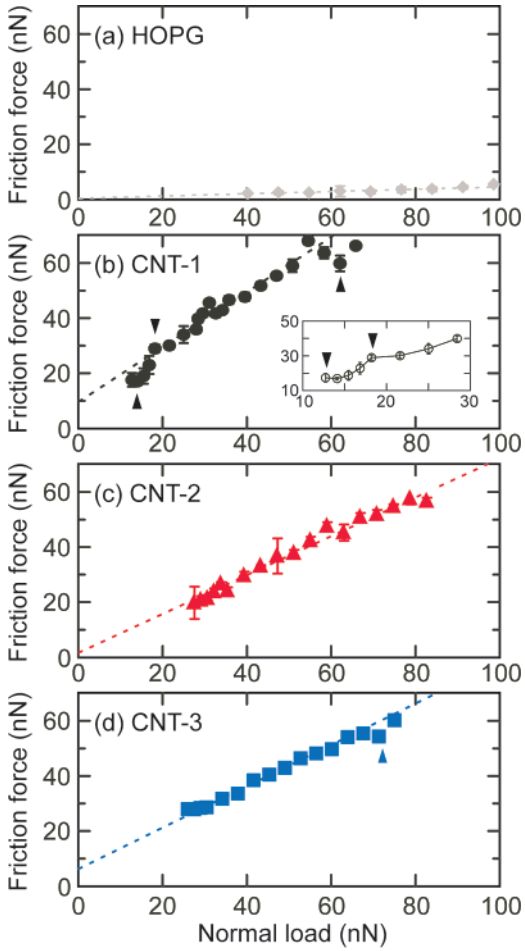

Figure 2. Friction vs normal load curves for (a) HOPG, (b) CNT-1, (c) CNT-2, and (d) CNT-3. The inset of Figure 2b represents the extension of a low load region.

We consider this structural flexibility of CNTs to be the origin of their characteristic frictional properties.

The friction force (F) is expressed as $F = \tau A_r$, where τ is the interfacial shear strength per unit area and A_r is the real area of contact. If the interfacial shear strength increases linearly with the local pressure $P = W/A_r$, then

$$\tau = \tau_0 + \alpha P \tag{1}$$

$$F = \tau_0 A_r + \alpha W \tag{2}$$

Therefore, effective coefficient of friction μ_{eff} is

$$\mu_{eff} = \alpha + \tau_0/P = \alpha + \tau_0 A_r/W \tag{3}$$

In the macroscopic system, μ_{eff} is independent of the normal load and macroscopic area because P is much greater than τ_0.[25] However, our experiment was done using AFM and the effect of P, that is, the effects of the normal load and the contact area, could not be disregarded. Because the length of the CNTs was not uniform, some of CNTs came into contact with the AFM tip at the normal load which was less than $W_{cr}N$, where W_{cr} is the critical buckling load of CNT and N is the number of CNTs contacted. In this case, A_r will

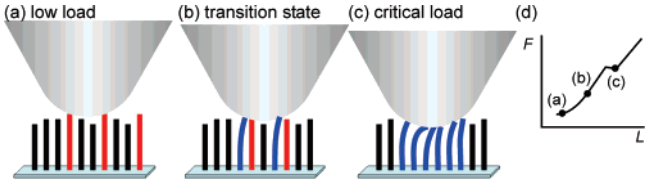

Figure 3. Schematics of the collapse process of CNT/SiC: (a) extremely low load; (b) normal load is less than critical buckling load; (c) critical buckling load; (d) schematics of corresponding load−displacement curve.

be proportional to N and be independent of the normal load. Therefore, the friction is proportional to the normal load. The schematic of this stage is shown in Figure 3a. In parts a−c of Figure 3, the red bars indicate CNTs contacting the AFM tip but not buckling. When the normal load exceeded $W_{cr}N$, the initially contacted CNT buckled. As a result, A_r was gradually increased when the normal load was increased because the shorter CNTs were able to contact the AFM tip. Therefore, the friction force increased nonlinearly with respect to the normal load. The schematic of this stage is shown in Figure 3b. In parts b and c of Figure 3, the blue bars indicate the contacted and buckled CNTs. Finally, all CNTs inside the contact area buckled and A_r became substantially constant. The friction force was increased linearly with respect to the normal load at this point. The schematic of this stage is shown in Figure 3c. The corresponding friction−normal load curve is shown in Figure 3d, and it was found to be very compatible with the inset of Figure 2b.

Here, the critical buckling load of each CNT is important to the nonlinear behavior of the friction. In general, W_{cr} of nanotubes for clamped-free loading was given by[26]

$$W_{cr} = (1/4)\pi^2 EI/L^2 \tag{4}$$

where E is the Young's modulus of the nanotube, $I = \pi R^4/4$ is the area momentum of inertia, L is the tube length, and R is the radius of nanotube. The values estimated for W_{cr} are 30 nN for CNT-1, 0.2 nN for CNT-2, and 0.6 nN for CNT-3. In our experiments, there were a few CNTs inside the contact area. For CNT-1, the order of W_{cr} was comparable to that of the normal load. Therefore, the nonlinear behavior of friction was observed at the low load region as shown in the inset of Figure 2b. On the other hand, for CNT-2 and CNT-3, W_{cr} was much smaller than the normal load. Therefore, the friction increased linearly with respect to the normal load. However, a sudden drop in the slope of the friction force curve was observed as shown in Figure 2d. According to a theoretical study,[7] some buckling modes have been predicted under axial compression, and each mode appears in response to the normal load. The sudden drop in the friction force curve that we observed would correspond to the change in the buckling structure.

The sudden decrease in the slope of the friction force−normal load curve was considered to be the signature of shell buckling, which indicates the collapsing process illustrated in Figure 3. For local buckling induced by axial compression,

the critical strain depends little on length and estimates to[7]

$$\epsilon_c = 4\sqrt{D/C}\, d^{-1} = \frac{2h}{d\sqrt{3(1-\nu^2)}} \quad (5)$$

where d, ν, and h are the diameter, the Poisson ratio, and the wall thickness of the nanotube, respectively. D and C indicate a flexural rigidity and the in-plane stiffness, respectively. On the basis of the standard relations,[27] D and C are represented as $Eh^3/12(1-\nu^2)$ and Eh, respectively. Here, E is the Young's modulus of the nanotube. With properly chosen tubule parameters, $\nu = 0.19$ and $h = 0.066$ nm,[7] one finds

$$\epsilon_c = (0.077\ \text{nm})d^{-1} \quad (6)$$

When bending, only one side of a tube is compressed and thus it can buckle. Assuming that it buckles when its local strain $\epsilon = Kd/2$, where K is the local curvature, is close to that in axial compression (eq 6), the critical curvature is estimated as

$$K_c = (0.155\ \text{nm})d^{-2} \quad (7)$$

In our experiment on CNT-1, d and L were 5 and 50 nm, respectively. Therefore, the critical bending angle $\theta_c = K_c L$ was estimated to be about 18°. Therefore, we estimated the displacement parallel to the surface due to the bending of the CNT to be about 15 nm.

Figure 4a shows the conformational change of CNT-1 depending on the normal load. In Figure 4a, the scan was repeated at the same position. The horizontal and vertical axes correspond to the position and time, respectively. Therefore, the image showed the change of the conformation of the CNTs from moment to moment. The normal load was varied as a sequence of 13 nN (I), 40 nN (II), and 13 nN (III) as shown in Figure 4a. Figure 4b shows the averaged height variation of each region. At a normal load of 13 nN, a nonflat cross section was observed because the length of the CNTs was not uniform. The conformation of the CNTs drastically changed when the normal load increased to 40 nN. The height variations were reduced at a high load of 40 nN. This result was compatible with the model that we suggested as shown in Figure 3. However, the cross sections of regions I and III were identical as shown in Figure 4b. Therefore, the conformation of CNTs did not change before and after the increment in the normal load. This result strongly suggested that the conformational change of the CNTs that we observed here was an elastic behavior. Furthermore, at each load, we observed lateral displacement of protrusions at about 20 nm in comparison with averaged height variations. The points indicated in Figure 4b correspond to the higher CNTs, which will be bent preferentially. This value was fairly consistent with the theoretically predicted value of 15 nm at the critical bending angle of CNT-1. Consequently, the sudden drop in the slope of the

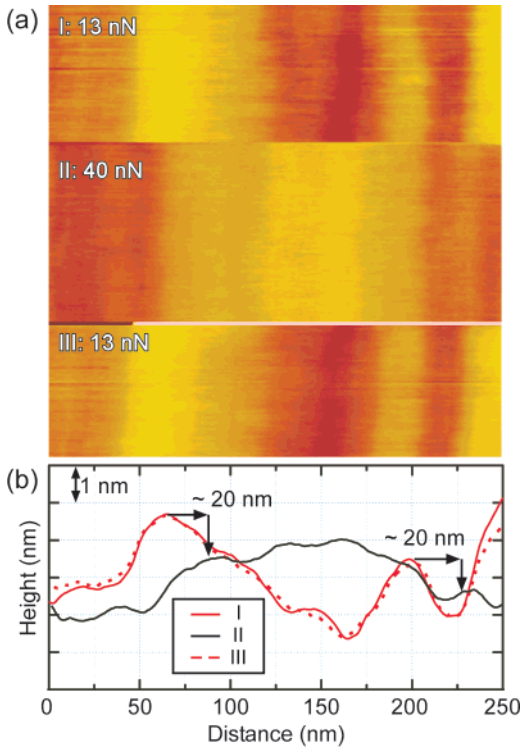

Figure 4. (a) Conformational change of CNT-1 depending on the normal load. A slow scan was performed from top to bottom. A fast scan from left to right was repeated at the same position. The normal load was varied as a sequence of 13 nN (I), 40 nN (II), and 13 nN (III). (b) The averaged height variation of each region.

friction force curve depending on the normal load is likely to be caused by the bending of the CNTs. In addition, in our experiments no change in the conformation of the CNTs was observed before and after the increment of the normal load. This is clearly indicated by the fact that the cross sections of regions I and III were identical as shown in Figure 4b. The contact pressure during the experiment was estimated to be about 1−3 GPa. Therefore, the CNT films did not peel even when they were rubbed hard with the AFM tip more than 100 times at a contact pressure of a few gigapascals. This result strongly supports the fact that CNT/SiC films have good wear resistance because of the covalently bonded VACNT films grown on the SiC substrate.

However, the slope of the friction force did not change before and after a singular point. Therefore, we expediently defined the coefficient of friction of the CNTs to be the slope of friction force−normal load curve. The apparent coefficients of friction of CNT-1, CNT-2, and CNT-3 were evaluated to be 1.0, 0.6, and 0.8, respectively. These values indicate that the thicker CNT exhibited a higher coefficient of friction, while the longer CNT exhibited a lower coefficient of friction force. In any case, all CNT/SiC films exhibited extremely high coefficients of friction (0.6−1.0) compared with the values for other carbon-based materials, such as HOPG (less than 0.1), C_{60}[21] (ultralow ~0), DLC[22] (less than 0.1), and CN_x[23] (0.2−0.4). The interesting properties of CNT/SiC, such as the nonlinearity of the friction force−normal load curve, high coefficient of friction, and good wear resistance, would make it possible to control the

frictional properties of these materials by changing the length and diameter of the CNT and the applied normal load. For these reasons, we consider CNT/SiC to be a promising candidate for high-friction and wear-resistant tribomaterials.

In summary, we evaluated the tribological properties of CNT/SiC using AFM. CNT/SiC exhibited characteristic frictional properties, such as nonlinearity of the friction force−normal load curve, high coefficient of friction, and good wear-resistant performance. We attributed the properties we observed to the intrinsic mechanical properties of CNTs, that is, the nonlinear elastic property caused by buckling. Furthermore, from the results of our evaluation of the apparent coefficient of friction, longer and thinner CNTs were found to have lower coefficients of friction. These results led us to conclude that CNT/SiC could be a promising candidate for high-friction and wear-resistant tribomaterials.

References

(1) Iijima, S. *Nature* **1991**, *354*, 56.
(2) Wong, E. W.; Sheehan, P. E.; Lieber, C. M. *Science* **1997**, *277*, 1973.
(3) Falvo, M. R.; Clary, G. J.; Taylor, R. M., II; Chi, V.; Brooks, F. P., Jr.; Washburn, S.; Superfine, R. *Nature* **1997**, *389*, 582.
(4) Iijima, S.; Brabec, C. J.; Maiti, A.; Bernholc, J. *J. Chem. Phys.* **1996**, *104*, 2089.
(5) Waters, J. F.; Guduru, P. R.; Jouzi, M.; Xu, J. M.; Hanlon, T.; Suresh, S. *Appl. Phys. Lett.* **2005**, *87*, 103109.
(6) Yap, H. W.; Lakes, R. S.; Carpick, R. W. *Nano Lett.* **2007**, *7*, 1149.
(7) Yakobson, B. I.; Brabec, C. J.; Bernholc, J. *Phys. Rev. Lett.* **1996**, *76*, 2511.
(8) Tracy, M. M. J.; Ebbesen, T. W.; Gibson, J. M. *Nature* **1996**, *381*, 678.
(9) Salvant, J.-P.; Kulik, A. J.; Bonard, J.-M.; Briggs, G. A. D.; Stöckli, T.; Méténier, K.; Bonnamy, S.; Béguin, F.; Burnham, N. A.; Forró, L. *Adv. Mater.* **1999**, *11*, 161.
(10) Yu, M.-F.; Files, B. S.; Arepalli, S.; Ruoff, R. S. *Phys. Rev. Lett.* **2000**, *84*, 5552.
(11) Walters, D. A.; Ericson, L. M.; Casavant, M. J.; Liu, J.; Colbert, D. T.; Smith, K. A.; Smalley, R. E. *Appl. Phys. Lett.* **1999**, *74*, 3803.
(12) Thostensona, E. T.; Renb, Z.; Choua, T. *Compos. Sci. Technol*. **2001**, *61*, 1899.
(13) Ajayan, P. M.; Schadler, L. S.; Giannaris, C.; Rubio, A. *Adv. Mater.* **2000**, *12*, 750.
(14) Ren, Z. F.; Huang, Z. P.; Xu, J. W.; Wang, J. H.; Bush, P.; Siegal, M. P.; Provencio, P. N. *Science* **1998**, *282*, 1105.
(15) Fan, S.; Chapline, M. G.; Franklin, N. R.; Tombler, T. W.; Cassell, A. M.; Dai, H. *Science* **1999**, *283*, 512.
(16) Murakami, Y.; Chiashi, S.; Miyauchi, Y.; Hu, M.; Ogura, M.; Okubo, T.; Maruyama, S. *Chem. Phys. Lett.* **2004**, *385*, 298.
(17) Hata, K.; Futaba, D. N.; Mizuno, K.; Namai, T.; Yumura, M.; Iijima, S. *Science* **2004**, *306*, 1362.
(18) Kinoshita, H.; Kume, I.; Tagawa, M.; Ohmae, N. *Appl. Phys. Lett.* **2004**, *85*, 2780.
(19) Dickrell, P. L.; Sinnott, S. B.; Hahn, D. W.; Raravikar, N. R.; Schadler, L. S.; Ajayan, P. M.; Sawyer, W. G. *Tribol. Lett.* **2005**, *18*, 59.
(20) Schwarz, U. D.; Zwörner, O.; Köster, P.; Wiesendanger, R. *Phys. Rev. B* **1997**, *56*, 6987.
(21) Miura, K.; Kamiya, S.; Sasaki, N. *Phys. Rev. Lett.* **2003**, *90*, 055509.
(22) Bhushan, B.; Dandavate, C. *J. Appl. Phys.* **2000**, *87*, 1201.
(23) Kato, K.; Umehara, N.; Adachi, K. *Wear* **2001**, *254*, 1062.
(24) Kusunoki, M.; Rokkaku, M.; Suzuki, T. *Appl. Phys. Lett.* **1997**, *71*, 2620.
(25) He, G.; Müser, M. H.; Robbins, M. O. *Science* **1999**, *284*, 1650.
(26) Gere; J. M.; Timoshenko, S. P. *Mechanics of Materials*; PWS-Kent: Boston, MA, 1984.
(27) Landau, L. D.; Lifshitz, E. M. *Elastic Theory*; Pergamon: Oxford, 1986.

NL0714482